Comparison of the high-pressure behavior of the cerium oxides Ce_2O_3 and CeO_2

M. J. Lipp,[1] J. R. Jeffries,[1] H. Cynn,[1] J.-H. Park Klepeis,[1] W. J. Evans,[1] D. R. Mortensen,[2] G. T. Seidler,[2] Y. Xiao,[3] and P. Chow[3]

[1]*Lawrence Livermore National Laboratory, Livermore, California 94550, USA*

[2]*Physics Department, University of Washington, Seattle, Washington 98195-1560, USA*

[3]*HPCAT, Geophysical Laboratory, Carnegie Institute of Washington, Argonne National Laboratory, Argonne, Illinois 60439, USA*

(Received 24 August 2015; published 9 February 2016)

The high-pressure behavior of Ce_2O_3 was studied using angle-dispersive x-ray diffraction to 70 GPa and compared with that of CeO_2. Up to the highest pressure Ce_2O_3 remains in the hexagonal phase (space group 164, $P\bar{3}2/m1$) typical for the lanthanide sesquioxides. A theoretically predicted phase instability for 30 GPa is not observed. The isothermal bulk modulus and its pressure derivative for the quasihydrostatic case are $B_0 = 111 \pm 2$ GPa, $B_0' = 4.7 \pm 0.3$, and for the case without pressure-transmitting medium $B_0 = 104 \pm 4$ GPa, $B_0' = 6.5 \pm 0.4$. Starting from ambient-pressure magnetic susceptibility measurements for both oxides in highly purified form, we find that the Ce atom in Ce_2O_3 behaves like a trivalent Ce^{3+} ion ($2.57\mu_B$ per Ce atom) in contrast to previously published data. Since x-ray emission spectroscopy of the $L\gamma$ ($4d_{3/2} \rightarrow 2p_{1/2}$) transition is sensitive to the $4f$ -electron occupancy, we also followed the high-pressure dependence of this line for both oxides up to 50 GPa. No change of the respective line shape was observed, indicating that the $4f$-electron configuration is stable for both materials. We posit from this data that the $4f$ electrons do not drive the volume collapse of CeO_2 from the high-symmetry, low-pressure fluorite structure to the lower-symmetry orthorhombic phase.

DOI: 10.1103/PhysRevB.93.064106

I. INTRODUCTION

Ce_2O_3 and CeO_2 are technologically important materials that are often encountered together in applications. Both can be considered as the two extreme brackets of CeO_x with x ranging from 1.5 to 2 where x can vary almost seamlessly over a wide range in between. They often occur together in reaction pathways that, e.g., eliminate pollutants, as in the use of ceria in catalytic converters, or allow thermochemical splitting of water into O_2 and H_2 possibly useful in the pursuit of energy storage [1–4]. The variability in x allows the material to either release or store oxygen and explains its great usefulness. Changing x from $x = 1.5$ to 2 results in a crystallographic structure change from a hexagonal lattice [space group (SG) 164, $P\bar{3}2/m1$, the so-called A type in the context of rare-earth sesquioxides with lattice constants $a = 3.891$ and $c = 6.059$ Å, one formula unit (f.u.) per cell [5]], to a face-centered cubic lattice (fluorite structure, SG 225, $Fm\bar{3}m$, $a = 5.411$ Å, four formula units per cell).

Since CeO_2 is thermodynamically stable there has been more research performed on it while relatively little is known about the less stable Ce_2O_3. Strangely enough, there appear to be more controversies surrounding CeO_2. One of them is caused by conflicting reports as to whether CeO_2 is paramagnetic [6,7] or diamagnetic [8]. Ce_2O_3, on the other hand, is definitely paramagnetic. While CeO_2 is thermodynamically stable, Ce_2O_3 converts into CeO_2 at ambient conditions, which allows experimental results of Ce_2O_3 to be affected by contamination with CeO_2 unless great care is exercised.

Part of the theoretical challenge of describing these materials lies in the coherent description of the f-electron configuration: f-electronic orbitals, bands, and their occupation [6,7,9–21]. Most research agrees that the Ce in Ce_2O_3 ought to have (about) one localized $4f$ electron while it is highly debated whether the $4f$ electron is completely delocalized in CeO_2 ($4f^0$ configuration, tetravalent) or whether a partial charge remains localized resulting in a mixed-valent configuration [6,7,9–17]. Early theoretical efforts found that CeO_2 would have 0.5 f electrons localized [10] and intermediate valence [14]. This was challenged by the results of an optical absorption experiment [6,7] which appeared to impose a limit of at most 0.05 localized f electrons in CeO_2, favoring a purely f^0 electronic configuration. The picture of a tetravalent Ce^{4+} ion in CeO_2 with a purely f^0 electronic configuration in the ground state might be too simplistic though [14,22], because the hole L in the oxygen $2p$ level interacts with the $4f$ resulting in a $4f^1L$ charge transfer configuration. More sophisticated approaches to treat both cerium oxides consistently become increasingly difficult to implement. A first-principles calculation of the solid-state properties of both CeO_2 and Ce_2O_3 had to distinguish between a core state model (CSM) for Ce_2O_3 localizing the f electron explicitly and a valence band model (VBM) delocalizing the f electron for CeO_2 [18]. Approaches employing screened hybrid density functionals appeared more promising in reproducing experimental results [21]. A later attempt using the local density approximation (LDA) allowed the description of both oxides at zero temperature and pressure by varying the so-called U parameter in the LDA + U formalism, which had to be set to 5–6 eV or higher for both Ce_2O_3 and CeO_2 [19,20]. The accuracy of the LDA + U approach was thought to provide a superior description of the cerium oxides [23].

Qi *et al.* expanded on the use of the LDA + U method and calculated the pressure dependence of structural parameters for Ce_2O_3 [24] as well as its elastic constants. Their work culminated in a prediction that the hexagonal structure of Ce_2O_3 would become unstable at 30 GPa [24], close to the pressure at which CeO_2 undergoes its own volume collapse from a high-symmetry fcc to a lower-symmetry orthorhombic phase. In CeO_2, the volume-collapse transition starts at 31 GPa and is completed at 38 GPa under nonhydrostatic conditions (no pressure-transmitting medium) [25]; under more

quasihydrostatic conditions (4:1 methanol-ethanol mixture), the transition continues for another 15 GPa [26]. The prediction of a structural instability in Ce_2O_3 is somewhat surprising, as the hexagonal structure of the sesquioxides is considered rather stable in other work [27]. For CeO_2, the theoretical data can be compared to results for lattice constants and bulk moduli of several experimental studies [25,26,28,29] whereas we are not aware of an equation of state study for Ce_2O_3 up to now.

Because the $4f$ electrons already have a large impact on the cerium oxides in their ambient state, our study focuses on the behavior of the $4f$ electrons under changing length scales by tuning the interatomic distances via pressurization in diamond anvil cells (DACs). For reference, in pure metallic cerium the f electrons drive the famous volume collapse from the γ to the α phase, which occurs at a pressure lower than 1 GPa [30], and for which the mechanism has been highly debated [31–33]. The same questions regarding localization and itinerancy, magnetic moments, their screening, and how this affects the volume evolution/collapse of metallic cerium also pertain to the behavior of CeO_2 and Ce_2O_3. In our present work we therefore investigate the pressure-volume (at room temperature) equation of state for Ce_2O_3 up to 70 GPa, the pressure dependence of its lattice constants as well as the bulk modulus B and its pressure derivative B'. We also examine the possibility that the thermodynamic instability of Ce_2O_3 leads to a disproportionation back into Ce metal and CeO_2 under pressure ($2Ce_2O_3 \rightarrow Ce + 3CeO_2$). Additionally, we characterize (at ambient pressure) our CeO_2 and Ce_2O_3 samples with regard to their magnetic susceptibility, which is intimately tied to their $4f$ occupancy. To assess the occupancy under pressures unattainable for magnetic susceptibility studies, we turn to x-ray emission spectroscopy of the $L\gamma$ line ($4d_{3/2} - 2p_{1/2}$) that exhibits a satellite due to an exchange interaction with a $4f$ electron [34,35] similarly to other rare-earth materials [36,37]. We compare our experimental observations of the $L\gamma$ line shape for Ce_2O_3 with those of metallic γ- and α-cerium, elemental lanthanum, and theoretical line shapes of Ce_2O_3 calculated previously by others in the framework of an Anderson impurity model with full multiplet couplings [34]. Finally, we estimate the $4f$-electron occupancy based on the integrated intensity of the $L\gamma$ satellite.

II. EXPERIMENTAL DETAILS

Measurements on CeO_2 were performed on a commercially acquired 99.9% CeO_2 powder (Alfa Aesar). Our Ce_2O_3 was synthesized starting from 99.9% cerium metal (Alfa Aesar) and CeO_2 that were weighed to give the correct stoichiometry, pressed into a pellet, and then heated to 1350°C for 10 h under ultra high pure argon flow. The resulting powder was golden-yellow in color, consistent with other reports of Ce_2O_3 synthesis (see Fig. 1) [38]. Ce_2O_3 is not thermodynamically stable: exposed to air at slightly elevated temperature it rapidly converts to CeO_2. This conversion apparently even proceeds when the material is stored in a bottle at room temperature. Indeed, our first experiments with a commercially acquired Ce_2O_3 sample had to be repeated with material produced in house, because the commercially acquired material was found, on subsequent analysis, to have changed into 80% CeO_2 (balance Ce_2O_3) over the years. Therefore, to prevent

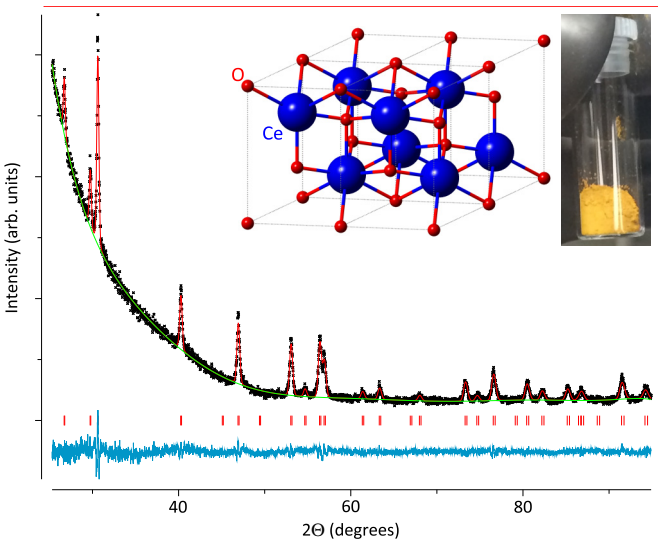

FIG. 1. X-ray diffraction (Cu $K\alpha$, 1.54059 Å) results at ambient conditions for our synthesis of Ce_2O_3. The black crosses are the data points, the green line is the background (with low-angle intensity dominated by the hermetically sealed holder), the tick marks are the Bragg peaks for the Ce_2O_3 structure, and the blue line at the bottom represents the difference between the data and the refinement. The refinement yielded an $R_{wp} = 5\%$. The crystal structure (left inset) is hexagonal, the so-called A type (SG 164) of the lanthanide sesquioxides. The right inset shows the golden-yellow color of Ce_2O_3 powder.

degradation and contamination, our Ce_2O_3 was synthesized and stored in an argon glovebox with less than 0.1 ppm of oxygen and less than 0.5 ppm or water present. A portion of the as-produced Ce_2O_3 powder was loaded into a hermetically sealed x-ray diffraction holder, and x-ray diffraction (see Fig. 1) indicated at least 99% purity; the lattice constants were 3.8908 and 6.0619 Å in excellent agreement with the literature [5]. In particular, no peaks indicative of the presence of CeO_2 were found in the freshly synthesized material.

Ambient-pressure magnetic characterization of the cerium oxides used a Quantum Design superconducting quantum interference device (SQUID) magnetometer with an applied field $H = 0.1$ T. Gel caps were used to contain the powders of both CeO_2 and Ce_2O_3. Great care was taken to limit any air exposure for the Ce_2O_3 sample: the powder was loaded into a gel cap and straw assembly inside of the glovebox, and that assembly was transferred within a sealed bag of argon to the magnetometer, where it was rapidly inserted in the helium atmosphere of the venting airlock.

Handling of the material and placing small crystallites into diamond anvil cells were performed in another glovebox. For the quasihydrostatic samples the DACs were additionally charged with neon as pressure-transmitting medium (PTM). We chose rhenium as gasket material for the angle-dispersive x-ray (ADX) diffraction experiments and used copper for pressure calibration [39]. Culet sizes of the diamonds ranged from 300 to 700 μm. Two DACs were prepared for the quasihydrostatic equation of state (EOS) experiments. The first one had tungsten as additional pressure marker (sample 1) and produced data ranging from 13 to 70 GPa; the second one

TABLE I. List of experiments.

Experiment	Conditions	Sample no.	Sample	Pressure-transmitting medium	Pressure marker	Pressure range (GPa)
EOS	Quasihydrostatic	1	Ce_2O_3	Neon	Cu, W	13–70
	Quasihydrostatic	2	Ce_2O_3	Neon	Cu	3.3–9
	Nonhydrostatic	3	Ce_2O_3		Cu	5.5–60
XES	Nonhydrostatic	4	Ce_2O_3		Ruby	0.3–50
	Nonhydrostatic	5	CeO_2		Ruby	0.0–48

(sample 2) with just copper as pressure marker was designed to fill in the low-pressure gap and delivered data from 3.3 to 9.0 GPa. The nonhydrostatic sample (sample 3) was loaded along with Cu as a pressure standard, and produced data from 5.5 to 60 GPa. For the x-ray emission spectroscopy (XES) experiments, we employed beryllium as the gasket material with ruby as pressure calibrant and loaded several samples investigating either CeO_2 or Ce_2O_3. Table I summarizes the different experimental setups.

ADX diffraction and XES experiments were carried out at the Advanced Photon Source at the High Pressure Collaborative Access Team (HPCAT) Sector 16 IDB and 16 IDD beamlines, respectively. The typical incident wavelength for ADX diffraction was ~0.4 Å. For the XES, we used high-energy x rays (11 or 18 keV) entering axially through the diamonds, and collected the $L\gamma$ x rays (from 6007 to 6090 eV, peak at 6052 eV) leaving through the beryllium gasket under a 90° angle to the incoming beam. The energy was scanned using a standard 4-in., spherically bent (333) Si analyzer crystal on a 1-m Rowland geometry situated at 90° to the incoming x-ray beam with a resolution of 1 eV.

III. RESULTS AND DISCUSSION

A. Ambient-pressure magnetic characterization of the Ce oxides

The temperature-dependent magnetic susceptibilities χ of the cerium oxides are shown in Fig. 2. Immediately evident is the magnitude of χ for Ce_2O_3 relative to that of CeO_2: the former exhibits a magnetic susceptibility that is at least 20 times larger than the latter over the entire temperature range. The solid lines through the data points for both oxides are fits to a modified Curie-Weiss expression:

$$\chi(T) = \chi_0 + f\frac{C}{T - \Theta_{CW}}, \quad (1)$$

where χ_0 is a constant susceptibility, f is the molar fraction of Ce, C is the Curie constant, and Θ_{CW} is the Curie-Weiss temperature.

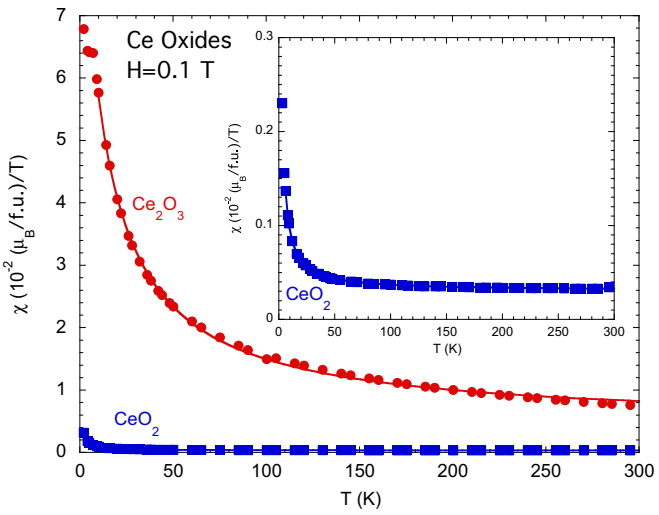

FIG. 2. Magnetic susceptibility in a 0.1 T magnetic field for Ce_2O_3 (red circles) and as-received CeO_2 (blue squares). The lines are fits to the sum of a Curie-Weiss law and a constant susceptibility (see text).

For Ce_2O_3, the results of this fit yield a full Ce^{3+} moment (measured $\mu_{eff} = 2.57\mu_B$ versus the expected Hund's rule value of $\mu_{eff} = 2.54\mu_B$), $\chi_0 = 4.5 \times 10^{-3}\,\mu_B$/f.u., and a $\Theta_{CW} = -12.5$ K, suggesting weak antiferromagnetic correlations between the Ce ions. The observed full, trivalent Ce moment is perhaps not surprising in Ce_2O_3, as the oxidation state would be expected to be Ce^{3+} ([Xe]$4f^1$). However, the measured effective moment is in contrast to the report of Pinto *et al.*, which suggested an effective Ce moment half the trivalent value [40]. Pinto *et al.* note that this low effective moment could be due to crystalline field effects, but another explanation could be the presence of CeO_2 impurities, as they are clearly evident from their published diffraction pattern. No evidence for magnetic ordering is seen in our temperature-dependent susceptibility data at $H = 0.1$ T.

While Ce_2O_3 may be expected to exhibit the classic trivalent rare-earth element moment, CeO_2 should be tetravalent (Ce^{4+}), with a filled outer-shell electron configuration ([Xe]) and thus a diamagnetic susceptibility. Indeed, Laachir *et al.* have reported a diamagnetic susceptibility for an ultrapure sample of CeO_2 (<6 ppm ferromagnetic impurities) [8], although no temperature dependence was included in their report. Our temperature-dependent magnetic susceptibility data for CeO_2, on the other hand, are best described by Eq. (1) with $\chi_0 = 3.0 \times 10^{-4}\,\mu_B$/f.u. (paramagnetic not diamagnetic) and a $\Theta_{CW} = 0$ K. The lack of obvious diamagnetism suggests that the picture of a $4f^0$ tetravalent Ce ion may be too simple of a description of CeO_2. The Curie tail seen in the susceptibility of CeO_2 is suggestive of the presence of impurities. If these impurities are assumed to be trivalent Ce ions, then application of Eq. (1) to our CeO_2 specimen implies that only about 0.5% of the Ce ions are Ce^{3+} rather than Ce^{4+}.

B. Ce_2O_3 crystal structure under pressure

Figure 3 shows selected angle-dispersive x-ray diffraction patterns for Ce_2O_3: (a) *nonhydrostatic* data from sample 3 (no pressure-transmitting medium), and (b) *quasihydrostatic* data for samples 1 and 2 [39]. Up to the highest pressure, both

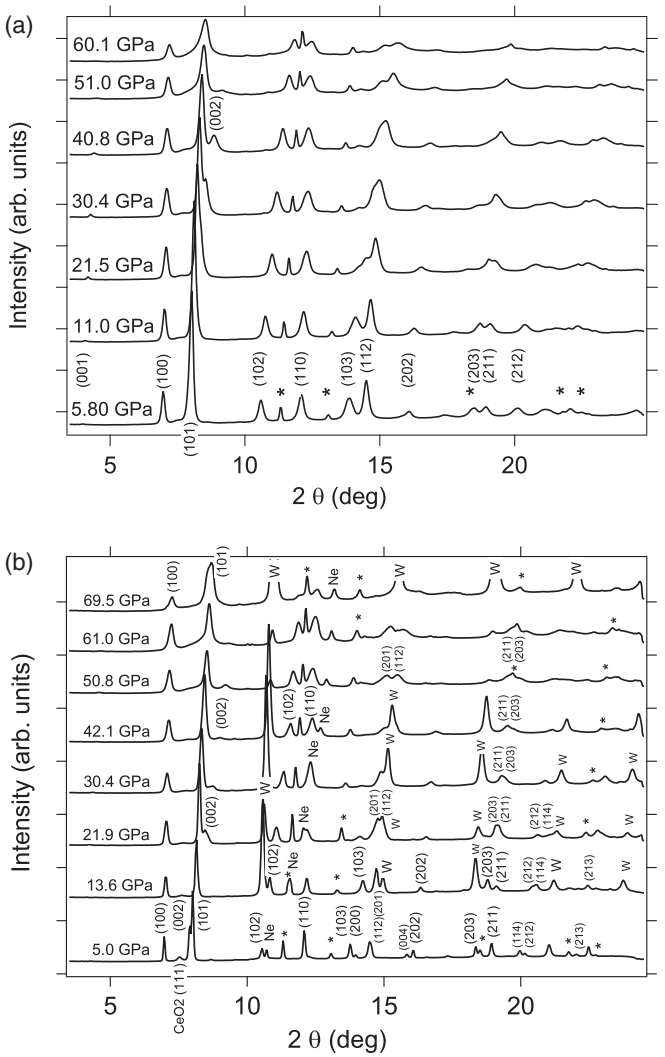

FIG. 3. (a) Angle-dispersive x-ray diffraction patterns of Ce_2O_3 under *nonhydrostatic* compression (sample 3) in the DAC at different pressures. Wavelength was 0.406626 Å. The pessure calibrant was copper (Cu peaks indicated by *). No pressure-transmitting medium was used. The (002) peak is overwhelmed by the (101) peak, and is not distinguishable until ∼30 GPa as a shoulder. (b) Angle-dispersive x-ray diffraction patterns of Ce_2O_3 under *quasihydrostatic* compression in the DAC at different pressures. Wavelength was 0.406626 Å. The (002) peak of Ce_2O_3 starts out to the left of the dominant (101) at low pressure and has switched over to the right at ∼20 GPa. The pressure calibrant was copper (Cu peaks indicated by *). The 5.0-GPa pattern (second sample) is free of W peaks. The other spectra (first sample) also contain diffraction peaks of W. The pressure-transmitting medium was neon; the (111) peak of neon is visible in all the patterns.

quasihydrostatic and nonhydrostatic samples remained in the hexagonal symmetry and the structure was consistent with that of $P\bar{3}2/m1$ (SG 164). After pressure release, the sample returned back to the literature values for lattice constants and volume within experimental uncertainty, which excludes a disproportionation of Ce_2O_3 into Ce and CeO_2 under pressure.

Figure 4 shows our measured lattice constants c and a for Ce_2O_3 up to 70 GPa. Figure 5 displays the quasihydrostatic

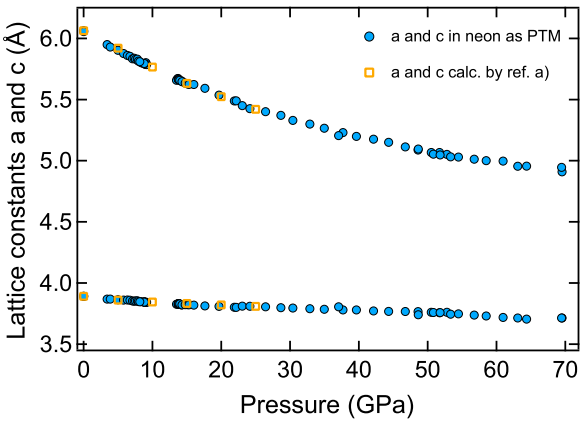

FIG. 4. Pressure dependence of the lattice constants a and c for Ce_2O_3 compressed quasihydrostatically with a neon pressure-transmitting medium. Ref. (a): [24].

and nonhydrostatic equations of state for Ce_2O_3. The Birch-Murnaghan equation of state

$$P(V) = \tfrac{3}{2}B_0(x^{7/3} - x^{5/3})\left[1 + \tfrac{3}{4}(B_0' - 4)(x^{2/3} - 1)\right]$$
$$\text{with } x = V_0/V \qquad (2)$$

was fitted to the EOS data. We find an isothermal bulk modulus $B_0 = 111 \pm 2$ GPa and the derivative of the isothermal bulk modulus $B_0' = 4.7 \pm 0.3$ for the quasihydrostatic data and $B_0 = 104 \pm 4$ GPa and $B_0' = 6.5 \pm 0.4$ for the nonhydrostatic case. Both EOSs are basically identical up to about 25 GPa, after which pressure the nonhydrostatic EOS diverges and becomes somewhat stiffer. Fitting results using the Vinet equation of state yield values of B_0 and B_0' that are within the uncertainties quoted above.

Qi *et al.* [24] calculated the lattice constants and equation of state using the LDA + U approach in the framework of density functional theory. Their predicted bulk modulus is $B_0 = 135$ GPa and its pressure derivative $B_0' = 3.96$ —quite different from our values—but their $p(V)$ data fit well onto the present isotherms (see Figs. 4 and 5). While their calculated

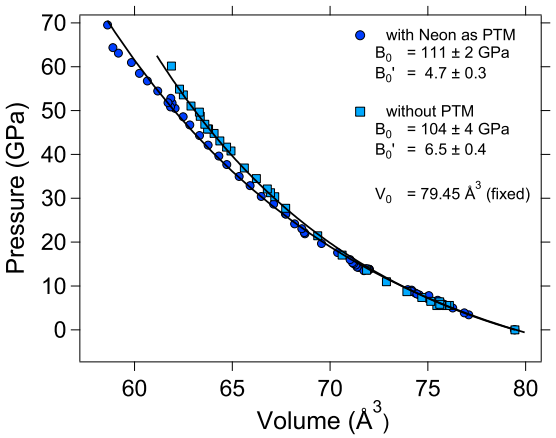

FIG. 5. Pressure-volume room-temperature isotherms (equation of state—EOS) for Ce_2O_3 under quasihydrostatic (with neon as PTM) and nonhydrostatic conditions. The zero-pressure volume was fixed at 79.45 Å^3 for both.

TABLE II. EOS parameters for Ce_2O_3 and CeO_2.

Compound	B (GPa)	B' (GPa)
Ce_2O_3		
Calc.[a,b,c,d] LDA + U	130; 144.7; 135; 150	–; –; 4.96; –
Calc.[c]	109 (VRH average)	
Calc.[d] LDA + DMFT	160	
Calc.[e,f] LDA (CSM)	165.8; 125.9	
Expt. Present work, Birch-Murnaghan EOS (quasihydrostatic)	111 ± 2	4.7 ± 0.3
Expt. Present work, Birch-Murnaghan EOS (nonhydrostatic)	104 ± 4	6.5 ± 0.4
CeO_2		
Calc.[a,b] LDA + U	214; 213.7	
Calc.[e] LDA (VBM)	214.7	
Calc.[g] screened hybrid density functional	206.1	
Expt. fcc / orthorhombic[h]	230 ± 10/304 ± 25	4.0/4.0
Expt. fcc[i]	236 ± 4	4.4 ± 0.4
	220 ± 9	4.4 ± 0.4
Expt. fcc[j]	204	

[a]Reference [19].
[b]Reference [20].
[c]Reference [24] Adiabatic bulk modulus K_S.
[d]Reference [43].
[e]Reference [18].
[f]Reference [27].
[g]Reference [21].
[h]Reference [25] Isothermal bulk modulus B_0, Birch-Murnaghan equation of state.
[i]References [26,29] Isothermal bulk modulus B_0, Birch-Murnaghan equation of state.
[j]Reference [28] Adiabatic bulk modulus K_S, obtained from elastic constants C_{11} and C_{12}.

B_0 is quite a bit higher than our measured one, they also propose an adiabatic bulk modulus $K_S = 109$ GPa based on a Voigt-Reuss-Hill (VRH) averaging scheme of their calculated elastic constants C_{ij} for polycrystalline material. The adiabatic and isothermal bulk moduli are related by the expression $K_S = B_0(1 + \alpha\gamma T)$, where α is the thermal expansion coefficient and γ is the Grüneisen parameter. While these values are not experimentally available for Ce_2O_3, they have been determined for the close relative Y_2O_3, where $\alpha_Y = 25 \times 10^{-6}$ K^{-1} and $\gamma_Y = 1.5$ (the subscript Y denotes that these data are for Y_2O_3 rather than Ce_2O_3) [41,42]. Using these values from Y_2O_3 implies that B_0 and K_S for Ce_2O_3 should be within about 1% of each other, suggesting that the VRH-derived bulk modulus of Qi *et al.* is more consistent with our experiments than the energy-derived bulk modulus. Furthermore, their calculated anisotropic behavior of the lattice constants at 25 GPa is $\Delta a/a \sim 1.9\%$ and $\Delta c/c \sim 10.5\%$. Experimentally, at 25 GPa, we find $\Delta a/a \sim 2.1\%$ and $\Delta c/c \sim 10.4\%$, in very good agreement. The anisotropy continues on: At 70 GPa we find that $\Delta a/a \sim 4.6\%$ whereas $\Delta c/c \sim 18.5\%$. In other words, most of the more than 25% volume reduction at 70 GPa originates from compression along the c axis under pressure. Table II contains a compilation of the present data and a comparison with theoretical calculations mostly based on the LDA + U formalism. The predictions for Ce_2O_3 show substantial variance while also presenting a larger bulk modulus than our measurements.

At 30 GPa, Qi *et al.* find an anomalously high bulk modulus (289 GPa) and a negative C_{44} elastic constant, implying a predicted structural change away from the hexagonal unit cell for pressures in excess of approximately 30 GPa. However, up to the highest pressure measured, the hexagonal structure persists experimentally. Determining whether this predicted phase transition is hindered by kinetic effects or finite-temperature entropic contributions will require additional theoretical work.

C. Persistent f-electron occupancy in Ce_2O_3 under pressure

Owing to Hund's rules, the $4f$ occupancy of the lanthanides manifests clear temperature-dependent behavior in the magnetic susceptibility, making these measurements sensitive probes of the f-electron configuration. However, the experimental capabilities to perform magnetic susceptibility under pressure typically do not exceed 2 GPa. We therefore use the satellite of the $L\gamma$ emission ($4d_{3/2} \rightarrow 2p_{1/2}$) following the excitation of a $2p$ electron into the continuum in Ce as a proxy for the presence of a localized $4f$ electron as has been done in numerous previous studies of other lanthanides [34–37,44]. The satellite is caused by the exchange interaction of the f electron with the $2p$ hole and therefore provides a simple

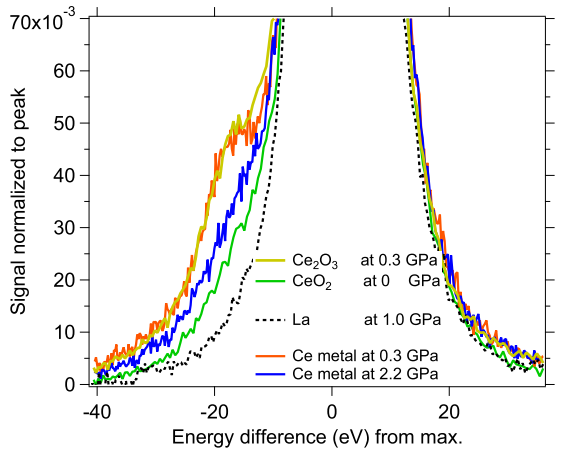

FIG. 6. X-ray emission spectra of the $L\gamma$ emission for Ce_2O_3, CeO_2, and La as well as metallic cerium at two different pressures—at 0.3 GPa below the 15% volume collapse and at 2.2 GPa above the volume collapse. With the exception of CeO_2 all samples were contained inside a DAC confined by a beryllium gasket.

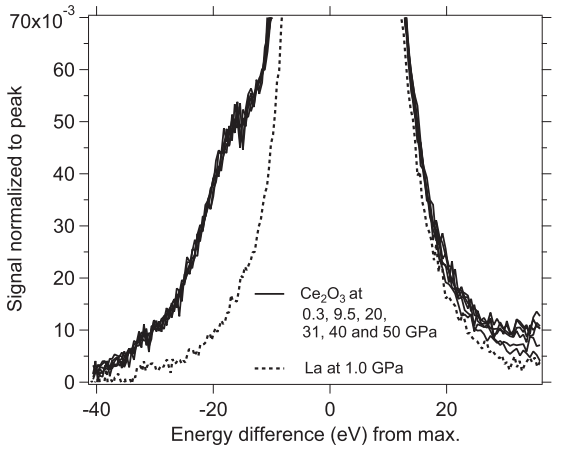

FIG. 7. $L\gamma$ emission spectra for Ce_2O_3 at pressures of 0.3, 9.5, 20, 31, 40, and 50 GPa (solid lines). Also shown is the line shape of the zero-f-electron element lanthanum. Within the experimental uncertainty the curves are indistinguishable from each other and do not change with pressure. The dip at -15 eV is an artefact.

answer as to whether a localized $4f$ electron exists [45]. The volume collapse in cerium metal from the γ to the α phase is accompanied by a significant reduction of the $L\gamma$ satellite [35] tracking the f occupancy closely [46], thus highlighting the utility of XES to track changes in the nature of the bonding of the f electrons.

Tanaka *et al.* [34] calculated the $4d \rightarrow 2p$ line shape of the $L\gamma$ radiation of Ce_2O_3 and found that it looked very similar to that of the Ce^{3+} ion where the lower-energy satellite can be assigned to the low-spin final state $(4d^9\ 4f^1)\ ^1P$. They determined that effects of the hybridization of the $2p$ valence band with the $4f$ orbitals are almost canceled out by "phase matching" of the involved wave functions, meaning that the hybridization affects both intermediate and final state in nearly the same manner [34,47] and the signature of an electronic charge redistribution between intermediate and final states does not appear [47]. Our experimental findings reveal that the actual line shape follows qualitatively the calculated one but differs in some detail. The experimentally observed line shapes are broader, similar to the way the observations of the line shapes of Ce metal are broader than the modified extended atomic calculations [35] since only a small number of orbitals are allowed to hybridize in the calculations.

In order to visualize changes in the f-electron occupancy, we show in Fig. 6 the $L\gamma$ emission of lanthanum, taken from a sample in a DAC at 1 GPa pressure. The La $L\gamma$ emission spectrum serves as our true zero f-electron system baseline, showing a lack of a satellite and providing a hallmark line shape for the main peak [47]. Additionally and for comparison, the spectra of Ce_2O_3 (at the low pressure of 1 GPa inside a DAC) and CeO_2 outside a DAC are included in Fig. 6. The long exposure times of several hours for these measurements required that Ce_2O_3 and La were sealed in a DAC to guard against their chemical reactivity. Figure 6 also shows the line shapes of cerium metal below and above the 15% volume collapse at 0.75 GPa, which coincides with a ~30% drop in f occupancy. Figure 6 shows that the line shape of cerium metal at 0.3 GPa is basically identical to the one of Ce_2O_3, the largest of the satellites. Other nominally trivalent cerium compounds (such as Ce_2S_3 and $CeSi_2$, not shown) also exhibit the same $L\gamma$ line shape.

The XES spectra of Ce_2O_3 under pressure are plotted in Fig. 7. Up to the highest pressure of 50 GPa, the satellite for Ce_2O_3 does not appear to change. The lack of changes under pressure shows that any changes in the bonding and thus in the EOS are not due to f-electron involvement, at least up to 50 GPa. As the XES line shapes are very similar for Ce_2O_3 and cerium metal (at ambient pressure), so are their respective f occupancies. Without being able to address the possibility of the magnetic moment generated by the $4f$ electron being screened by the $5d$ band electrons, as in the case for cerium metal, and thus affecting the value of the magnetic susceptibility, we can say that localized f electrons in Ce_2O_3 do persist under pressure. Ce_2O_3 thus represents a material with a stable $4f$-electron occupancy (trivalent) and crystal structure up to at least 50 GPa.

D. CeO_2 under pressure

Unlike Ce_2O_3, CeO_2 does not retain its ambient-pressure crystal structure up to very high pressures. Instead, and near 30 GPa, CeO_2 undergoes an fcc-orthorhombic phase transition with an accompanying volume collapse of nearly 10%, comparable in size to the isostructural collapse of Ce metal [30]. Figure 8 shows a comparison of the normalized equations of state of Ce_2O_3 and CeO_2 through its volume collapse together with previous results by other authors. At low pressures Ce_2O_3 is more compressible than CeO_2, but with increasing pressure CeO_2 makes up for the lack in volume change when it undergoes its volume collapse from the fcc to the orthorhombic phase [25,26]. Whether the f electrons of CeO_2 play a role in the volume collapse, as is the case for Ce metal, has been an open question.

While Ce_2O_3 showed a small satellite similar in magnitude to that of Ce metal (Fig. 6), the line shape of CeO_2 reveals an even smaller satellite intensity. We know of no calculations

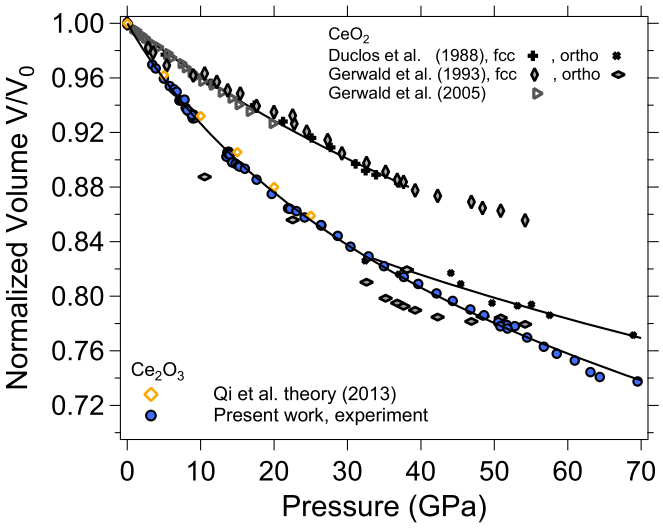

FIG. 8. Comparison of the normalized EOSs for Ce_2O_3 and CeO_2. The data by Duclos *et al.* [25] were taken without PTM, the data by Gerwald *et al.* with a PTM (4:1 methanol-ethanol mixture [26] in 1993, and a 16:3:1 methanol-ethanol-water mixture [29] in 2005). The Ce_2O_3 data (theory) by Qi *et al.* are from [24].

of the $L\gamma$ line shape for CeO_2 but it can be compared to the experimentally observed line shape of La. La possesses no $4f$ electron and its line shape shows no satellite (see Fig. 6). Comparing the La line shape with the one of CeO_2, a small, remnant satellite in CeO_2 is apparent (see Fig. 6). This remnant can be modeled with the same line shape parameters as Ce_2O_3 or Ce metal but with reduced amplitude.

XES spectra for CeO_2 under pressure are shown in Fig. 9. Up to the highest pressure of 48 GPa, and identical to the behavior of Ce_2O_3, the satellite intensity does not appear to change. This pressure range encompasses the structural transition in CeO_2 from the high-symmetry fluorite fcc to the

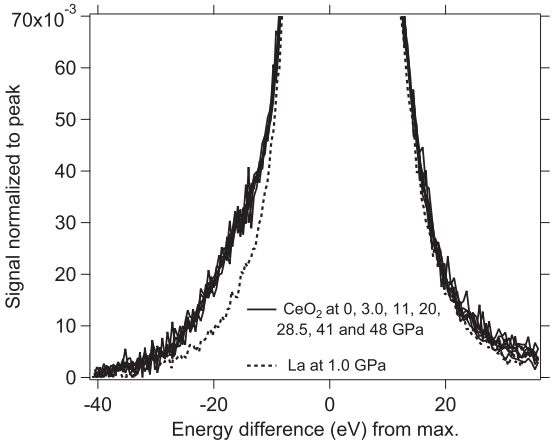

FIG. 9. $L\gamma$ emission spectra for CeO_2 at pressures of 0, 3.0, 11, 20, 28.5, 41, and 48 GPa (solid lines). The line shape of the zero-f-electron element lanthanum is again displayed for comparison. Within the experimental uncertainty the curves are indistinguishable from each other and as for Ce_2O_3 there is no discernible change with pressure.

low-symmetry orthorhombic phase, which starts at ~31 GPa and is completed at 38 GPa in nonhydrostatic conditions [25]. The persistence of the small satellite in the $L\gamma$ emission of CeO_2 suggests that the volume collapse from the high-symmetry fcc to the low-symmetry orthorhombic phase is not driven by changes in the f-electron configuration, through either delocalization or hybridization.

Assuming that the relationship with the f-electron occupancy also holds for the satellite area of CeO_2, one can estimate the number of f electrons for both oxides. Correlating the satellite area of cerium metal at pressures below the volume collapse (γ-Ce) with an f-electron occupancy of 0.97 [46], one finds $n_f \sim 1.09 \pm 0.1$ for Ce_2O_3 and $n_f \sim 0.35 \pm 0.05$ for CeO_2 (note: this value is larger than the upper limit, 0.005, of impurity Ce^{3+} ions as determined from magnetic susceptibility). The nonzero value of n_f for CeO_2 indicates that the Ce ions cannot be modeled by a simple closed-shell picture lacking f electrons. The extracted values of n_f are lower than recent hybrid density functional calculations, which find $n_f = 1.31$ for Ce_2O_3 and $n_f = 0.80$ for CeO_2 [21], but compare well with bond valence methods finding $n_f = 0.27$ for CeO_2 and $n_f = 1$ for Ce_2O_3 [48]. Less recent calculations in the framework of the Anderson impurity model with a filled valence band give a range of $0.38 < n_f < 0.52$ for CeO_2 and $n_f \sim 1$ for Ce_2O_3 [49]. Reference [11] finds an f occupancy of about 0.6 for CeO_2 via $3d$ core level photoemission, and an older calculation [10] finds 0.5.

IV. CONCLUSION

While the physical properties depend heavily on whether the $4f$ electron is approximately localized (Ce_2O_3) or more delocalized (CeO_2), the volume reduction of cerium oxides under pressure is unlikely explained by changes in the $4f$-electron configuration. In fact, based on our observation of the satellite feature in the $L\gamma$ line shape, the properties of the $4f$ electrons do not change with pressure, at least up to 50 GPa. In particular, the volume collapse in CeO_2 from the high-symmetry fcc structure to the low-symmetry orthorhombic—playing out over a range of ~10 GPa starting at 31 GPa—is not caused by a change in the $4f$-electron behavior. Previous XES experiments and calculations on cerium metal have established that the area of the satellite structure follows the ground state moment and occupancy rather closely [35,46]. It is therefore argued that Ce_2O_3 possesses ~1.09 localized f electrons and $CeO_2 \sim 0.35$.

ACKNOWLEDGMENTS

This work was performed under the auspices of the U.S. Department of Energy by Lawrence Livermore National Laboratory under Contract No. DE-AC52- 07NA27344. Portions of this work were performed under Laboratory Directed Research and Development (Grant No. LDRD 14-ERD-041). G.T.S. acknowledges support by the U.S. Department of Energy, Basic Energy Sciences under Grant No. DE-FG02-09ER16106 and also by the Office of Science, Fusion Energy Sciences and the National Nuclear Security Administration through Grant No. DE-SC0008580. Portions of this work were performed at HPCAT (Sector 16), Advanced Photon Source

(APS), Argonne National Laboratory. HPCAT operations are supported by DOE-NNSA under Award No. DE-NA0001974 and DOE-BES under Award No. DE-FG02-99ER45775, with partial instrumentation funding by NSF. The Advanced Photon Source is a U.S. Department of Energy (DOE) Office of Science User Facility operated for the DOE Office of Science by Argonne National Laboratory under Contract No. DE-AC02-06CH11357.

[1] M. S. Dresselhaus and I. L. Thomas, Nature (London) **414**, 332 (2001).
[2] S. Abanades and G. Flamant, Solar Energy **80**, 1611 (2006).
[3] W. C. Chueh, C. Falter, M. Abbott, D. Scipio, P. Furler, S. M. Haile, and A. Steinfeld, Science **330**, 1797 (2010).
[4] N. V. Skorodumova, S. I. Simak, B. I. Lundqvist, I. A. Abrikosov, and B. Johansson, Phys. Rev. Lett. **89**, 166601 (2002).
[5] H. Bärnighausen and G. Schiller, J. Less-Common Met. **110**, 385 (1985).
[6] P. Wachter, in *Valence Instabilities*, edited by P. Wachter and H. Boppart (North-Holland, Amsterdam, 1982), p. 145.
[7] F. Marabelli and P. Wachter, Phys. Rev. B **36**, 1238 (1987).
[8] A. Laachir, V. Perrichon, A. Badri, J. Lamotte, E. Catherine, J. C. Lavalley, J. E. Fallah, L. Hilaire, F. Le Normand, E. Quérémé, G. N. Sauvion, and O. Touret, J. Chem. Soc., Faraday Trans. **87**, 1601 (1991).
[9] E. Wuilloud, B. Delley, W.-D. Schneider, and Y. Baer, Phys. Rev. Lett. **53**, 202 (1984).
[10] D. D. Koelling, A. M. Boring, and J. H. Wood, Solid State Commun. **47**, 227 (1983).
[11] A. Fujimori, Phys. Rev. B **28**, 2281 (1983).
[12] A. Bianconi, A. Kotani, K. Okada, R. Giorgi, A. Gargano, A. Marcelli, and T. Miyahara, Phys. Rev. B **38**, 3433 (1988).
[13] T. K. Sham, R. A. Gordon, and S. M. Heald, Phys. Rev. B **72**, 035113 (2005).
[14] A. Fujimori, Phys. Rev. B **27**, 3992 (1983).
[15] H. Dexpert, R. C. Karnatak, J. M. Esteva, J. P. Connerade, M. Gasgnier, P. E. Caro, and L. Albert, Phys. Rev. B **36**, 1750 (1987).
[16] G. Kaindl, G. Schmiester, E. V. Sampathkumaran, and P. Wachter, Phys. Rev. B **38**, 10174 (1988).
[17] H. Ogasawara, A. Kotani, K. Okada, and B. T. Thole, Phys. Rev. B **43**, 854 (1991).
[18] N. V. Skorodumova, R. Ahuja, S. I. Simak, I. A. Abrikosov, B. Johansson, and B. I. Lundqvist, Phys. Rev. B **64**, 115108 (2001).
[19] D. A. Andersson, S. I. Simak, B. Johansson, I. A. Abrikosov, and N. V. Skorodumova, Phys. Rev. B **75**, 035109 (2007).
[20] C. Loschen, J. Carrasco, K. M. Neyman, and F. Illas, Phys. Rev. B **75**, 035115 (2007).
[21] P. J. Hay, R. L. Martin, J. Uddin, and G. E. Scuseria, J. Chem. Phys. **125**, 034712 (2006).
[22] K. O. Kvashnina, S. M. Butorin, and P. Glatzel, J. Anal. At. Spectrom. **26**, 1265 (2011).
[23] J. L. F. Da Silva, Phys. Rev. B **76**, 193108 (2007).
[24] Y.-Y. Qi, Z.-W. Niu, C. Cheng, and Y. Cheng, Front. Phys. **8**, 405 (2013).
[25] S. J. Duclos, Y. K. Vohra, A. L. Ruoff, A. Jayaraman, and G. P. Espinosa, Phys. Rev. B **38**, 7755 (1988).
[26] L. Gerward and J. S. Olsen, Powder Diffr. **8**, 127 (1993).
[27] M. Rahm and N. V. Skorodumova, Phys. Rev. B **80**, 104105 (2009).
[28] A. Nakajima, A. Yoshihara, and M. Ishigame, Phys. Rev. B **50**, 13297 (1994).
[29] L. Gerward, J. S. Olsen, L. Petit, G. Vaitheeswaran, V. Kanchanad, and A. Svane, J. Alloys Compd. **400**, 56 (2005).
[30] D. C. Koskenmaki and K. A. Gschneidner, Jr., *Handbook on the Physics and Chemistry of Rare Earths* (North-Holland Publishing Company, Amsterdam, 1978), Chap. 4, p. 337.
[31] B. Johansson, Philos. Mag. **30**, 469 (1974); Phys. Rev. B **11**, 2740 (1975).
[32] J. W. Allen and R. M. Martin, Phys. Rev. Lett. **49**, 1106 (1982).
[33] M. Lavagna, C. Lacroix, and M. Cyrot, Phys. Lett. A **90**, 210 (1982).
[34] S. Tanaka, H. Ogasawara, A. Kotani, and K. Okada, J. Phys. Soc. Jpn. **64**, 2225 (1995).
[35] M. J. Lipp, A. P. Sorini, J. Bradley, B. Maddox, K. T. Moore, H. Cynn, T. P. Devereaux, Y. Xiao, P. Chow, and W. J. Evans, Phys. Rev. Lett. **109**, 195705 (2012).
[36] B. R. Maddox, A. Lazicki, C. S. Yoo, V. Iota, M. Chen, A. K. McMahan, M. Y. Hu, P. Chow, R. T. Scalettar, and W. E. Pickett, Phys. Rev. Lett. **96**, 215701 (2006).
[37] G. Fabbris, T. Matsuoka, J. Lim, J. R. L. Mardegan, K. Shimizu, D. Haskel, and J. S. Schilling, Phys. Rev. B **88**, 245103 (2013).
[38] C. M. Hamm, L. Alff, and B. Albert, Z. Anorg. Allg. Chem. **640**, 1050 (2014).
[39] H. Cynn, B. J. Baer, S. G. MacLeod, W. J. Evans, M. J. Lipp, J. P. Klepeis, Z. Jenei, J. Y. Chen, K. Catalli, D. Popov, and C. Y. Park, *Bulletin of the American Physical Society*, APS March Meeting 2012, http://meetings.aps.org/link/BAPS.2012.MAR.V25.7; they reported a Vinet EOS with $V_{at}(\mathrm{Cu}) = 47.2299\ \mathrm{\AA}^3$, $B_0 = 133.41$ GPa, and $B_0' = 5.3298$.
[40] H. Pinto, M. H. Mintz, M. Melamud, and H. Shaked, Phys. Lett. A **88**, 81 (1982).
[41] X. Cao, J. Mater. Sci. Technol. **23**, 15 (2007).
[42] H. A. Badehian, H. Salehi, and M. Ghoohestani, J. Am. Ceram. Soc. **96**, 1832 (2013).
[43] B. Amadon, J. Phys.: Condens. Matter **24**, 075604 (2012).
[44] J.-P. Rueff and A. Shukla, Rev. Mod. Phys. **82**, 847 (2010).
[45] F. de Groot and A. Kotani, *Core Level Spectroscopy of Solids* (CRC Press, Boca Raton, 2008).
[46] J.-P. Rueff, J.-P. Itié, M. Taguchi, C. F. Hague, J.-M. Mariot, R. Delaunay, J.-P. Kappler, and N. Jaouen, Phys. Rev. Lett. **96**, 237403 (2006).
[47] K. Jouda, S. Tanaka, and O. Aita, J. Phys.: Condens. Matter **9**, 10789 (1997).
[48] E. Shoko, M. F. Smith, and R. H. McKenzie, Phys. Rev. B **79**, 134108 (2009).
[49] T. Nakano, A. Kotani, and J. C. Parlebas, J. Phys. Soc. Jpn. **56**, 2201 (1987).